Astronomical Techniques and Instruments, Vol. 3, November 2026, 475–484

Article Open Access

Localization and radiation analysis of interference sources based on UAV platform

Hongrui Zhang[1], Liang Dong[2*], Lesheng He[1], Qiang Xi[2], Shengyang Li[3], Bin Tian[3], Ning Zhang[4], Mudi Li[2], Yifeng Qin[1]

[1]*School of Information*, *Yunnan University*, *Kunming* 650500, *China*

[2]*Yunnan Observatories*, *Chinese Academy of Sciences*, *Kunming* 650011, *China*

[3]*Yunnan Radio Monitoring Center*, *Kunming* 650228, *China*

[4]*Urumqi Monitoring Station of State Radio Monitoring Center*, *Urumqi* 830011, *China*

*Correspondence: dongliang@ynao.ac.cn

Received: December 1, 2025; Accepted: April 9, 2026; Published Online: April 10, 2026; https://doi.org/10.3724/ati2025091; https://cstr.cn/32083.14.ati2025091

© 2026 Editorial Office of Astronomical Techniques and Instruments, Yunnan Observatories, Chinese Academy of Sciences. This is an open access article under the CC BY-NC-ND 4.0 license (http://creativecommons.org/licenses/by-nc-nd/4.0/)

Citation: Zhang, H. R., Dong, L., He, L. S., et al. 2026. Localization and radiation analysis of interference sources based on UAV platform. *Astronomical Techniques and Instruments*, **3**(6): 475−484. https://doi.org/10.3724/ati2025091.

Abstract: With the widespread use of 5G, low-power, and WiFi wireless devices, radio telescopes are facing increasingly severe interference. These telescopes are usually constructed in areas with complex terrain, making it difficult to accurately locate hidden interference sources using conventional methods and complicating troubleshooting. To address this, we propose an interference source localization and electromagnetic analysis system based on an unmanned aerial vehicle platform, aiming to accurately determine the location of interference sources and their radiation distribution in two-dimensional space. The system uses a spatial multi-baseline switching function based on an airborne circular five-antenna array and a microwave switch matrix. High-precision intersection localization of interference sources is achieved through multi-baseline coherent interferometry, with a localization angle accuracy better than 5°. In terms of electromagnetic situation analysis, the system combines the flight trajectory of the unmanned aerial vehicle to record signal strength and position information in real-time, and generates an electric field strength distribution map. This not only helps to accurately determine the location of the interference source but also effectively assesses the scope of its impact on the radio telescope. Field test verification demonstrates that the system can provide robust data support for interference source identification, localization, and the planning and management of radio protection zones in radio astronomy operations, thereby significantly enhancing the efficiency and accuracy of interference source troubleshooting.

Keywords: Unmanned aerial vehicle; Interferometric direction finding; Signal source localization; Electromagnetic situation; Radiation analysis

1. INTRODUCTION

Radio telescopes are important astronomical observation tools that capture radio waves from celestial bodies to study celestial phenomena such as galaxies, black holes, pulsars, and solar activity, as well as their evolutionary laws. In radio astronomy observations, received signals are often extremely weak[1]. With the rapid development of modern communication technologies and the scarcity of radio frequency spectrum resources, radio astronomical observations are facing an increasing amount of artificial much interference, which seriously affects the quality and accuracy of observations.

Through research on the localization and troubleshooting of interference sources, the goal is to detect and locate these sources, further eliminate them, identify and reduce such interferences, thereby improving the reliability of observation data and ensuring the normal conduct of radio astronomical observation work.

In recent years, extensive research has been undertaken on interference source localization methods. In 2020, Zhao et al.[2] proposed a wireless localization algorithm based on Time Difference of Arrival (TDOA) and Received Signal Strength Indicator (RSSI) data fusion. This algorithm optimizes multiple initial position estimates, weighted using signal reception strength, improving the localization accuracy by approximately 20%. In 2022, Zhang et al.[3] proposed an intelligent radio interference monitoring method to meet the demand for high-sensitivity observations of the Five-hundred-meter Aperture

Spherical radio Telescope (FAST). This technique combines multi-station collaborative spectrum sensing with TDOA-based localization technology to achieve effective identification and accurate localization of interference signals. The adaptive filter used can effectively suppress interference signals by approximately 30 dB. Zhu et al.[4] proposed a localization algorithm based on joint time-frequency difference analysis, to address the interference of high-elevation satellites on radio astronomical observations. Simulation results show that the minimum localization error can be as low as 78 m for interference sources at an altitude of 300 km.

To improve the accuracy of interference source localization, Li[5] designed a six-channel phase interferometer direction-finding system in 2021. To address the problems of ambiguous azimuth angles and inconsistent amplitude-phase characteristics among channels, he proposed a high-precision direction-finding ambiguity resolution algorithm and a multi-channel amplitude-phase error correction method. Simulation results were used to verify the feasibility of this method for resolving ambiguity. In 2022, Memarian & Majidi[6] proposed a direction-finding method, using a uniform circular array as the reference directional element and an additional central omnidirectional element, building on the coherent interferometer. This method significantly improved the performance and accuracy of Direction of Arrival (DOA) estimation in scenarios involving multiple coherent or non-coherent signal sources and multipath environments. In the same year, Han & Gao[7] proposed an optimal estimation method for multi-baseline interferometers. Based on the principle of probability theory, this method weights the direction-finding results of different baselines and draws an analogy between this method and the idea of Kalman filtering, verifying its effectiveness. Liu et al.[8] addressed the shortcomings of existing detection methods for the quiet zones of the surrounding electromagnetic environment in radio astronomical observations and proposed a radio interference monitoring method using a four-antenna linear array. In relatively open and quiet environments, this four-antenna array can effectively identify the incoming direction of interference signals, with a reliability of approximately 87% for measurement angle errors not exceeding 5°.

However, in practical scenarios, the terrain around radio telescope sites is relatively complex, mostly in sparsely populated mountainous areas. The obstruction by mountain bodies affects signal propagation[9], which restricts the existing interference source detection and coverage analysis due to the influence of the geographical environment and multipath effects, resulting in poor actual troubleshooting results for interference sources hidden in the terrain. Additionally, handheld monitoring and direction-finding methods consume significant human and time costs.

In recent years, the application scope of Unmanned Aerial Vehicle (UAV) technology has been continuously expanding. Existing studies have applied UAVs to low-altitude electromagnetic environment monitoring to ensure the safe low-altitude operation of general aviation[10]. Introducing UAV technology into spatial electromagnetic detection represents a brand-new approach.

In view of the aforementioned difficulties in troubleshooting radio interference sources at radio telescope sites, UAVs provide an efficient solution for spatial electromagnetic detection, demonstrating significant advantages in interference source localization and radiation analysis. Airborne signals benefit from reduced multipath effects during propagation, enhancing stability and minimizing errors caused by signal reflection. Moreover, UAVs overcome terrain-related accessibility issues, reaching locations with complex topography that are otherwise inaccessible to personnel and vehicles. The mobility of UAVs also enables rapid interferometric and intersection measurements during flight, allowing precise localization of interference sources hidden in concealed areas, such as building interiors or vegetation. Additionally, UAVs offer flexibility in regional radiation analysis through two-dimensional spatial movement and position recording, facilitating real-time collection of spatial electromagnetic field data to determine the distribution of electromagnetic radiation intensity within the flight area.

Considering the advantages of UAV platforms, we introduce an interference source localization and radiation analysis system, based on a UAV platform developed by the research team. This system integrates a module for electromagnetic environment monitoring and direction finding on the UAV platform, and uses coherent interferometric direction-finding technology to achieve precise localization of interference sources. It takes advantage of the flexibility and maneuverability of UAVs in combination with an intersection localization strategy to accurately determine the location of interference sources.

In addition, the system also has a spatial radiation collection function. During the UAV's flight, it can record the electromagnetic radiation intensity of the corresponding space along the flight path in real time and draw an electromagnetic situation map, thereby clarifying the radiation impact range of the interference source. This function not only improves the system's ability to monitor and locate interference sources but also provides strong data support for the identification, localization, and management of interference sources.

2. INTRODUCTION TO THE TEST PLATFORM

This system comprises monitoring and direction-finding equipment, a UAV platform, a remote controller, and a monitoring Personal Computer (PC) terminal, as shown in Fig. 1. The monitoring and direction-finding devices consist of an antenna array, a monitoring and direction-finding module, and a digital signal processing board. The module is connected to the processing board via Radio Frequency (RF) and Low Voltage Differential Signaling

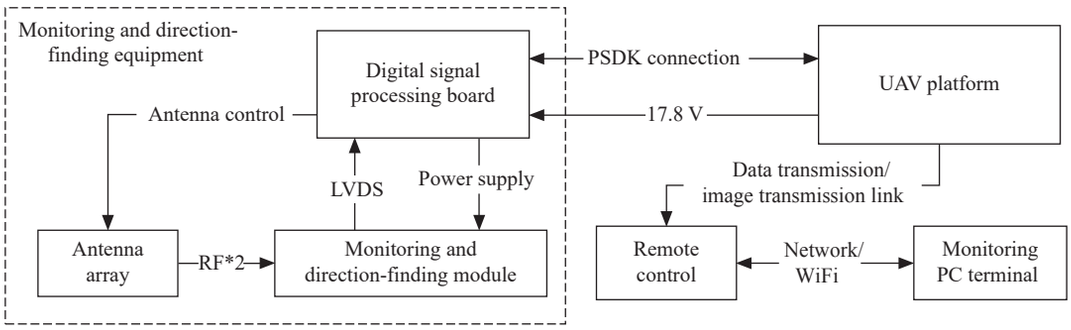


Fig. 1. The airborne monitoring equipment consists of an antenna array, a monitoring and direction-finding module, and a signal processing board.

(LVDS) links, and is powered by the processing board. The entire airborne system is supplied with 17.8 V power by the UAV platform and interfaces with the platform through the Payload Software Development Kit (PSDK) port. In addition, the UAV transmits the processed data and images to the remote controller and monitoring PC terminal via a dedicated wireless communication link.

The system has two main functions. One is interference source direction-finding, in which interference signals are collected by the antenna, then the positioning of the interference source is determined using coherent interference direction-finding technology and an intersection positioning method. The other is electromagnetic situation analysis, which uses the flexibility of the UAV and integrates its geolocation capability to test and store interference signal levels within the flight area. Subsequently, the flight trajectory is integrated to form a spatial electromagnetic situation map that determines the influence range of the interference source.

2.1. Hardware Composition of the System

2.1.1. *UAV platform*

The UAV platform used in the system is the DJI Mavic 3E. This UAV platform has a maximum take-off weight of 1.05 kg, a maximum ascent and descent speed of 6 m s^{-1}, a maximum horizontal flight speed of 15 m s^{-1}, and a maximum flight range of 32 km. It features high integration and good stability, which can meet the requirements of most interference source detection tasks.

The UAV platform consists of two parts: the UAV main body and the onboard payload. Among them, the UAV main body is composed of a power supply module, a detection module, a control unit, and a drive module. Except for the monitoring and direction-finding module in the external mounting, which is developed in this paper, all other components are provided by the DJI Mavic 3E. The overall structure of the UAV platform is shown in Fig. 2.

Our system contains several components, with specific

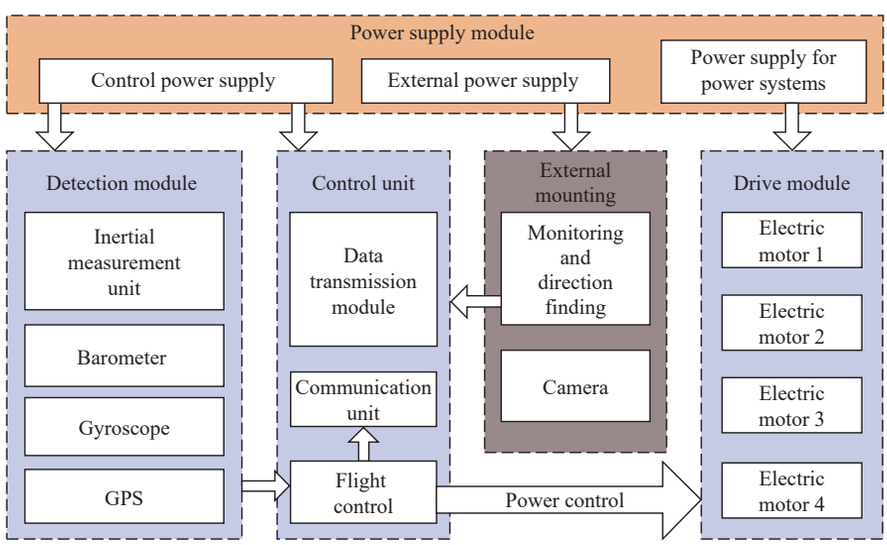


Fig. 2. Overall architecture of the UAV platform. The system is composed of a power supply module, a detection module, a control unit, an external mounting module, and a drive module. The power supply module provides control power and external power to the entire system. The detection module integrates an inertial measurement unit, a barometer, a gyroscope, and a GPS for flight status monitoring. The control unit consists of a flight control core, a communication unit, and a data transmission module, where the flight control unit sends power control signals to the drive module and receives sensor data from the detection module. Additionally, the external mounting module includes monitoring and direction-finding equipment as well as a camera for operational tasks.

functions. The power supply module consists of a control power supply, external power supply, and power source, and provides power to the detection module, control unit, external mounting, and drive module. The detection module includes an Inertial Measurement Unit (IMU), a barometer, a gyroscope, and a Global Positioning System (GPS) device, serving to determine the UAV's attitude measurement, altitude detection, and positioning, while also recording key flight information. The control module comprises a flight control unit, a communication unit, and a data transmission unit. Here, the flight control unit calculates the current attitude and generates corresponding control information for the drive module, the communication unit collects test information from external payloads such as cameras and monitoring & direction-finding modules, and the data transmission unit transmits information to the ground station for observation and storage. Additionally, the drive module consists of four motors, where the power supplied is regulated by the control module to provide appropriate flight power for the UAV.

2.1.2. *External payload*

The payload system incorporates two primary components, a high-resolution camera and a monitoring and direction-finding system. The camera includes a 4/3-inch Complementary Metal-Oxide-Semiconductor (CMOS) wide-angle sensor with 20 million pixels and a mechanical shutter, supporting high-speed continuous shooting at 0.7 s intervals to effectively avoid the "jello effect". It supports the connection of a Real Time Kinematic (RTK) module to achieve centimeter-level high-precision positioning. Complementing the visual payload, the monitoring and direction-finding system comprises a receiver and a 5-element antenna array, with its aerial structure shown in Fig. 3. This system operates within a receiving frequency range of 100 MHz to 6 GHz, enabling comprehensive spatial electromagnetic detection.

In Fig. 3, SP2T and SP4T refer to Single-Pole Two-Throw and Single-Pole Four-Throw microwave switches, respectively. The SP2T is responsible for the antenna selection function, choosing the corresponding antenna from A, B, C, D, and E to receive signals; the SP4T is responsible for the signal path allocation function, distributing the selected signal to the corresponding signal processing channel. The microwave switches are controlled by signals output from the digital signal processing board. Specifically, the RF channel RF 1 can select array elements A and B as inputs, while the RF channel RF 2 can select array elements B, C, D, and E as inputs. Therefore, there are 7 combinations of RF inputs, as shown in the truth table (Table 1). Here, vc 1, vc 2, and vc 3 are the control voltage signals sent by the digital signal processing board. vc 2 is responsible for controlling the SP2T switch, and vc1 and vc3 are responsible for controlling the SP4T switch. In addition, "0" represents a low level, and "1" represents a high level. By using these 7 antenna combinations, a phase difference matrix is obtained. Then, coherence analysis is performed based on the existing sample data, achieving high-precision direction finding of the interference source.

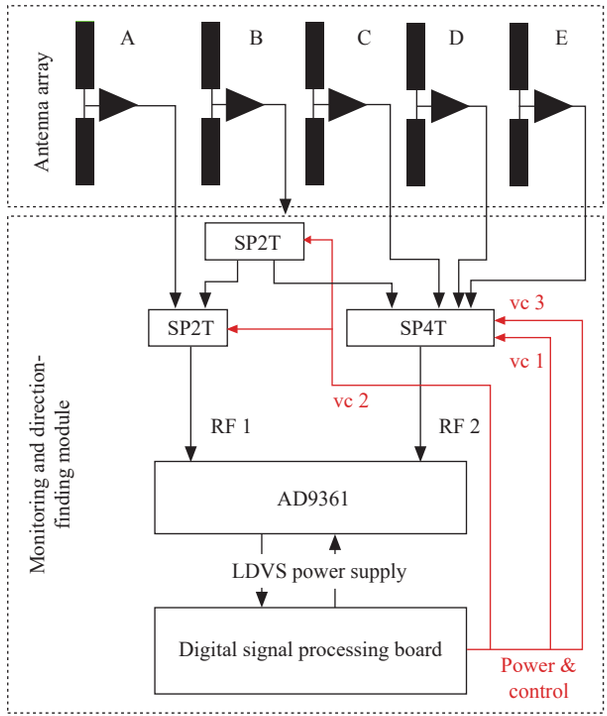


Fig. 3. Hardware architecture of the RF front-end module. The system employs a five-element Antenna Array (A−E) to receive external RF signals, which are initially routed to SP2T and SP4T RF switches for signal conditioning and channel selection. The conditioned signals are then fed into the AD9361 integrated transceiver chip, which facilitates bidirectional LVDS data streaming with the Digital Signal Processing Board and distributes internal control voltages (vc 1, vc 2, vc 3) to the switching circuitry, to manage the signal paths.

Table 1. Truth table for RF input, showing the 7 possible combinations of antenna element selections for RF channels RF 1 and RF 2, which are configured by the control voltage signals vc 1, vc 2, and vc 3. Here, "0" and "1" represent low and high logic levels, respectively, that govern the switching states of the SP2T and SP4T microwave switches, thereby defining the active channels for the direction-finding system

vc 1	vc 2	vc 3	RF 1	RF 2
0	0	0	A	C
0	0	1	A	D
0	1	0	B	C
0	1	1	B	D
1	0	0	A	E
1	0	1	A	B
1	1	0	B	E

The AD9361 chip receives, amplifies, and frequency-converts the RF analog signals filtered by the front-end switch network, and converts them into digital signals. These digital signals are output to the digital signal processing board via the LVDS interface for subsequent analysis.

The direction-finding antenna array, used for collecting spatial electromagnetic signals, adopts a five-element dual-hammerhead antenna array structure model, as

shown in Fig. 4. The positions of the antennas are uniformly distributed in terms of direction, and the directional gain range within the system's receiving frequency range is ±1.5 dBi.

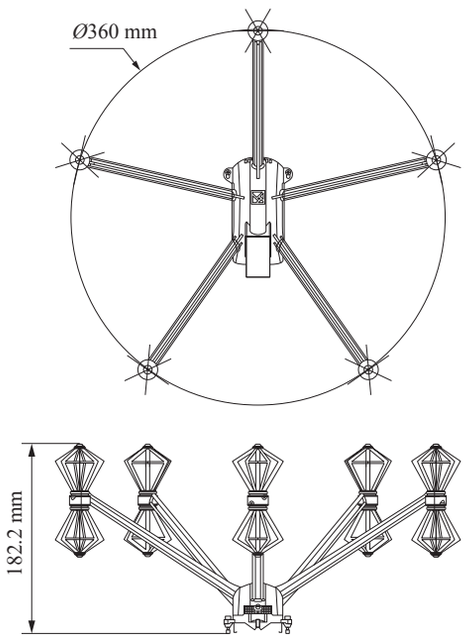


Fig. 4. Structural diagram of five-element antenna array.

2.2. Monitoring and Direction-finding Signal Acquisition and Processing Method

2.2.1. *Direction-finding platform data link*

The system operation block diagram is shown in Fig. 5. Among them, the aerial component includes the UAV and the integrated monitoring and direction-finding module carried by the UAV; the ground station component includes the remote controller and the monitoring PC terminal. In the monitoring and direction-finding module, RF 1 and RF 2 are the output ports of the antenna array, and AD9361 is a software-defined RF transceiver chip. It supports a wide frequency range from 70 MHz to 6 GHz and provides a configurable digital interface, which simplifies integration with the processor.

In the data receiving process, signals received by the antenna array first pass through a band-pass filter and an amplifier before being input into the AD9361 chip via two RF channels. This chip uses zero-IF receiving technology to process Intermediate Frequency (IF) signals, converting the high-frequency analog inputs into zero-IF signals through In-phase/Quadrature (IQ) mixing[11]. Subsequently, these signals are sampled and converted into digital signals by an Analog-to-Digital Converter (ADC), which are then transmitted via the LVDS interface to the digital signal processing board for coherent interference direction-finding and positioning, to determine the relative direction of the interference source. The digital signal processing board then transmits the processed data back to the UAV platform through the PSDK interface for further analysis. Finally, the ground station, comprising the UAV platform's remote controller and a monitoring computer terminal, receives RF digital signals via the data transmission/video transmission link for storage and further processing, while concurrently maintaining a local area network connection between the remote controller and the monitoring computer, to enable real-time viewing of the UAV status.

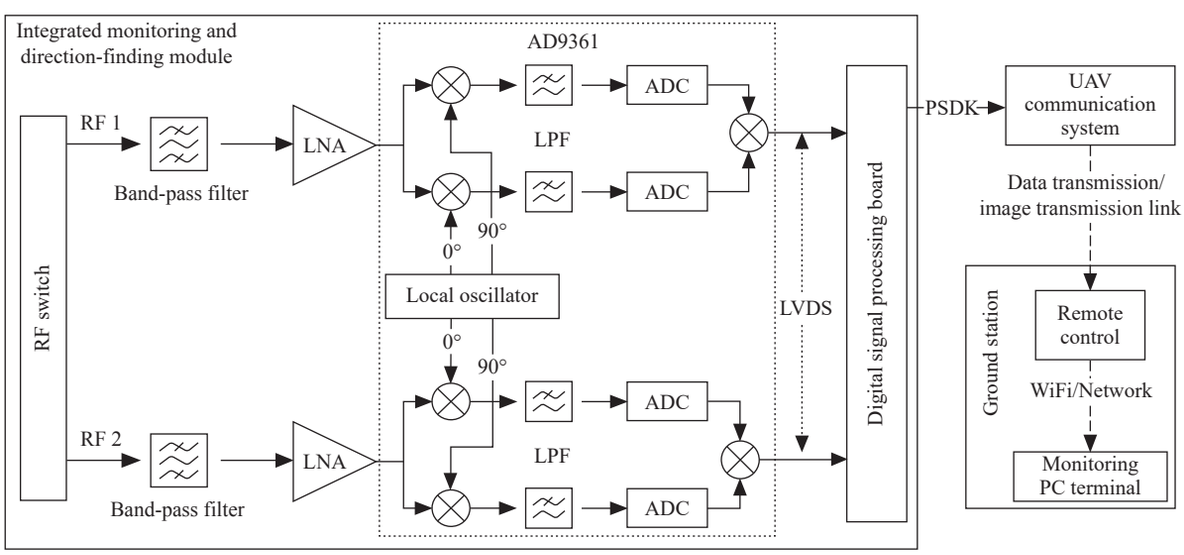


Fig. 5. Hardware architecture of the integrated monitoring and direction-finding module. The system receives external RF signals through an RF switch, which are then processed via two parallel channels (RF 1 and RF 2). Each channel consists of a band-pass filter and a low-noise amplifier (LNA) for signal conditioning. The conditioned signals are subsequently digitized by the AD9361 integrated circuit. Within the AD9361, the signals undergo I/Q down-conversion using a local oscillator, Low-Pass Filtering (LPF), and an ADC. The digital signals are then transmitted to the digital signal processing board via LVDS for further analysis. Finally, the processed data is sent to the Ground Station using the PSDK and WiFi/Network links, for remote monitoring and control.

2.2.2. *Principle of coherent interference direction-finding*

The coherent interferometer direction-finding algorithm is widely used in military and civilian direction-finding system architectures, thanks to advantages such as high direction-finding accuracy and adaptability to various antenna array structures[12]. Conventional interferometric direction-finding is based on acquisition of the incident wave phase distribution by antenna array elements, finding the direction by measuring the phase difference between the voltages received by each antenna array element. The interferometric direction-finding principle of the two-element antenna array is illustrated in Fig. 6A. The geometric model calculates the phase difference based on the wave path difference ($L\sin\theta$) caused by the incident angle θ and the antenna spacing L. The received signals are processed through digital receivers and a phase detector to perform incident angle analysis.

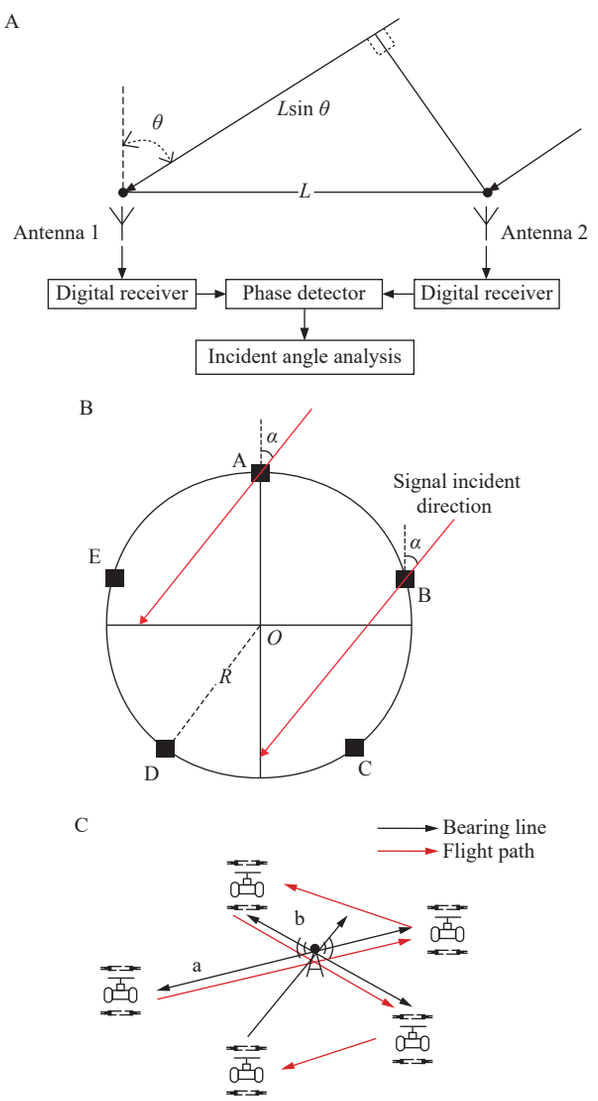


Fig. 6. Core direction-finding and positioning diagram of the system. (A) Schematic diagram of the two-element antenna array interferometric direction-finding principle. (B) Top-down simplified model of a 5-element uniform circular array. (C) Schematic diagram of the relationship between flight path and bearing line.

When a plane wave with frequency f (wavelength $\lambda = c/f$, where c is the speed of light) arrives at two direction-finding antennas (Antenna 1 and Antenna 2) spaced by a distance L from a direction forming an included angle θ with the antenna boresight, the phase difference φ (in radians) between the signals received by the two antennas is

$$\varphi = \frac{2\pi L}{\lambda}\sin\theta\,. \tag{1}$$

After performing the angle transformation, the incident angle of the plane wave is calculated as

$$\theta = \arcsin\left(\frac{\varphi\lambda}{2\pi L}\right). \tag{2}$$

After obtaining the phase difference φ of the two signals through a phase detector, the incident angle of the plane wave can be calculated.

However, in practical applications, there is mutual coupling between antenna array elements, and the antenna bracket may cause distortion and deformation of the wavefront. Such situations often reduce the direction-finding accuracy[13]. Therefore, to improve the direction-finding accuracy, the system in this paper adopts a multi-baseline five-element antenna array for coherent interference direction-finding. Specifically, the incident direction is determined by comparing the similarity between the acquired incident wave phase distribution and the azimuth and incoming wave phase distribution of the existing original samples.

The direction-finding model is shown in Fig. 6B, where A, B, C, D, and E represent receiving array elements, which are uniformly distributed on a circle with radius R. Black squares show element positions. It is assumed that a signal with frequency f is incident parallel to the antenna array elements, and α is the incident direction of the interference signal.

The switching of antenna pairs is automatically and sequentially completed by the digital signal processing board through control voltages (vc 1, vc 2, vc 3). The switching frequency depends on the required signal processing gain and the tracking requirements for dynamic signals. Within one positioning measurement cycle, the system traverses the seven antenna combinations listed in Table 1 within the millisecond scale to collect phase difference data of all baselines. The whole process is automatic without manual intervention. After the UAV flies to the predetermined direction-finding point, the system automatically executes the above process and outputs the results. Path planning is mainly used to guide the UAV to different direction-finding points for subsequent intersection positioning.

When antennas A and B start collecting data, the

receiver is connected to antenna elements A and B, and the phase difference ϕ_{BA} between antennas A and B can be obtained by reading the phase difference output by the phase detector. By changing the array elements connected to RF 1 and RF 2, the phase difference matrix can be derived by

$$\boldsymbol{\phi} = [\phi_{BA}, \phi_{CA}, \phi_{DA}, \phi_{EA}, \phi_{CB}, \phi_{DB}, \phi_{EB}]. \quad (3)$$

Then, the coherence coefficient ρ between the phase difference matrix $\boldsymbol{\phi}$ and the data sample $\phi_{(f,\alpha)}$ is calculated, as shown in Equation (4):

$$\rho = \frac{\boldsymbol{\phi} \times \phi_{(f,\alpha)}}{\sqrt{\boldsymbol{\phi}^2 \times \phi_{(f,\alpha)}^2}}. \quad (4)$$

Finally, the sample data $\phi_{\max(f_0,\alpha_0)}$ corresponding to the maximum coherence coefficient $\rho_{\max}$ is selected. The α_0 corresponding to the frequency f_0 of this sample data is the test result of the azimuth angle. Based on this, the incident direction of the plane wave is determined, and a direction-finding line is drawn, thereby providing a basis for interference source positioning.

2.2.3. *Implementation of intersection positioning*

As the direction parameter is one of the most reliable parameters of the target signal source, the direction-finding cross positioning method is the earliest developed, most studied, and most widely used passive positioning method[14]. This algorithm mainly uses the azimuth angle information of the target signal source measured at different geographical locations to obtain corresponding positioning direction-finding lines, and then determines the position of the target signal source through mathematical and geometric principles. Since the intersection positioning method requires direction-finding of the interference source at multiple locations, the high mobility of the UAV provides convenient advantages for intersection positioning. The intersection positioning process in this system is shown in Fig. 6C. The red arrows denote the flight paths of the UAVs, and the black arrows represent the bearing lines pointing toward the target UAVs. The UAV flies according to the incident angle while continuously monitoring the electric field intensity during flight. If the electric field intensity first increases and then decreases along the flight path, it indicates that the UAV has passed the interference source, and direction-finding will be performed again subsequently. The intersection point formed by two or more flight paths such as *a* and *b* corresponds to the position of the interference source.

The UAV interference source positioning process begins by setting the receiver to the target interference frequency to obtain an initial direction-finding line (line *a*). Subsequently, the UAV flies along this bearing while monitoring field strength. On detecting a peak where the strength shifts from increasing to decreasing, the operator manually hovers the drone to reacquire the direction-finding line. Next, the UAV rotates by a specific angle, flies straight for a set distance, hovers again, and conducts another test to derive a second direction-finding line (line *b*). Finally, this procedure is repeated to generate multiple direction-finding lines that converge at a single intersection point, achieving precise localization of the interference source.

3. FIELD TEST VERIFICATION AND ERROR ANALYSIS

During the field experiment, a signal source was used to simulate the interference source to be located, The signal source consists of a programmable signal generator, Keysight N5172B, equipped with a dipole antenna. After an on site investigation and analysis, Nongke Village, Pixian District, Chengdu City, was selected as the experimental verification site.

Following the confirmation that nearby power and network cables would not affect the test and that the area was not a no-fly zone, we placed an interference source at a concealed location. Subsequently, the UAV platform was utilized to conduct two primary analyses: first, performing intersection positioning to determine the source's coordinates and verify positional accuracy, and second, testing the interference radiation response at the specific frequency to generate an electromagnetic situation map and delineate the influence range of the interference source.

3.1. Intersection Positioning Test

To test the direction-finding accuracy of the UAV, the interference source was first placed at different orientations relative to the system. Subsequently, the test results were compared with the actual reference angles, and some of the obtained test results are shown in Table 2, where the 0° direction is defined as the heading of the UAV. A single-frequency continuous-wave (CW) signal is transmitted during the test. The test results are obtained by manually setting the signal source to transmit sequentially at different frequency points and performing direction-finding point by point, so as to evaluate the system performance at different frequencies.

The test data for all interference source directions were plotted into the error graph shown in Fig. 7.

We conclude that the direction-finding accuracy of our system is better than 5°, giving it excellent interference source positioning capability. Furthermore, when the orientation of the interference source is unknown, the intersection positioning method can be used to locate the position of the interference source. When multiple direction-finding lines stably intersect at the same point, the interference position can be obtained, using the single-station multi-point intersection positioning function. Fig. 8A shows the test process and results of the position interference source. During the test of the 1401.1 MHz interference source, the UAV took off on-site, obtained the

Table 2. Partial results of direction-finding accuracy test

Direction of interference source	0°		45°		90°	
Frequency/MHz	Direction line/(°)	Error/(°)	Direction line/(°)	Error/(°)	Direction line/(°)	Error/(°)
1100.1	356.8	−3.2	44.8	−0.2	88.8	−1.2
1200.1	359.0	−1.0	44.7	−0.3	88.6	−1.4
1300.1	1.7	1.7	44.3	−0.7	88.5	−1.5
1400.1	359.8	−0.2	43.8	−1.2	88.0	−2.0
1500.1	0.3	0.3	45.0	0.0	88.9	−1.1
1600.1	358.2	−1.8	45.0	0.0	88.9	−1.1
1700.1	358.1	−1.9	42.7	−2.3	88.8	−1.2
1800.1	358.1	−1.9	41.9	−3.1	89.3	−0.7
1900.1	359.4	−0.6	41.2	−3.8	90.3	0.3
1999.1	359.8	−0.2	43.5	−1.5	88.7	−1.3
Average error	−0.9		−1.3		−1.1	

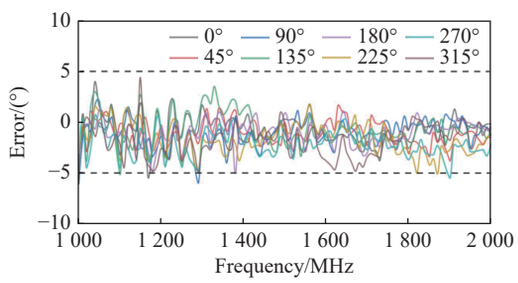


Fig. 7. Test the azimuth error of the system for interference source localization. The actual angular interval between the placed interference sources in the test is 45°.

approximate direction of the interference source via testing, and then drew the interference source direction-finding line. The relative position of the UAV was changed multiple times to draw direction-finding lines, obtaining the precise position of the interference source. In this test, the actual longitude and latitude of the interference source were (E103.799798°, N30.813690°), and the measured longitude and latitude were (E103.799771°, N30.813708°), with a measurement error of approximately 4 m.

3.2. Spatial Electromagnetic Situation Analysis and Testing

A spatial electromagnetic situation map analysis can check the influence range of a given interference source. Therefore, in this test, the transmission frequency of the signal source was set to 1501.1 MHz and the transmission power to 1 W, which were used as the test objects for analysis. The test distance interval was 20 m, the test altitude was 35 m, and the radiation analysis covered an area of approximately 0.33 km^2 (approximately 640 m in length and 520 m in width). The UAV's flight path and test results are shown in Fig. 8B. To accurately locate ground targets, the system adopts an annular progressive approximation flight strategy, using a flight trajectory of a set of concentric circles centered on the target. Starting from an initial distance, the UAV flies sequentially along circular flight paths with gradually decreasing radii. During each circular flight, the airborne radio frequency direction-finding system continuously scans the target signal and calculates the direction-finding angle. Through this periodic circular flight, the system can continuously collect direction-

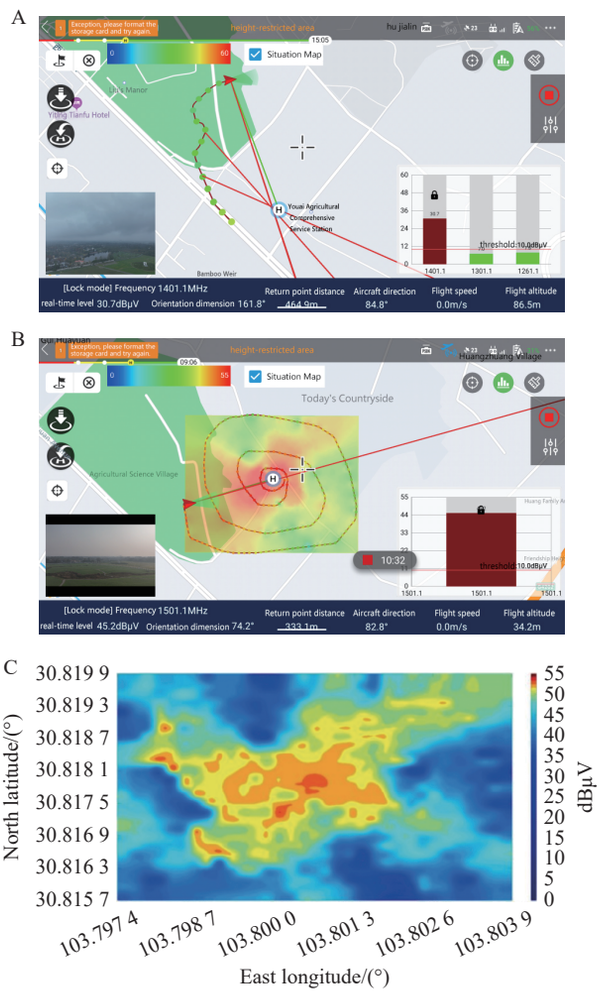


Fig. 8. Screenshots and results of the UAV field strength measurement experiment. (A) Screenshot of the UAV ground station monitoring interface. The map displays the real-time flight trajectory (green dashed line) and orientation of the UAV, along with red bearing lines showing the direction of the interference source. The right-side panel monitors real-time field strength, showing a current level of 30.7 dBμV against a threshold of 10.4 dBμV, while the bottom bar provides key telemetry data including frequency (1401.1 MHz), aircraft altitude (86.5 m), and flight speed. (B) Electromagnetic situation diagram during testing. Point H is both the UAV's take-off position and the location of the interference source. (C) Map of the electromagnetic field strength distribution in the experimental area.

finding data from different directions, gradually converge, and accurately estimate the target position using triangulation positioning or filtering algorithms. Meanwhile, the stable control of flight altitude and speed ensures the continuity and reliability of data collection. This strategy effectively overcomes the uncertainty of single-point direction-finding and achieves continuous improvement of positioning accuracy with the flight process, using path planning.

In the results of this test, the interference level in the central area reached 54.6 dBμV, and the minimum measured interference level was 34 dBμV. The electromagnetic situation map is based on these raw data, created using a spatial interpolation algorithm on the longitude, latitude, and field strength data collected at discrete points (i.e., actual UAV measurement points). This allows us to estimate the field strength values in the regions between measurement points, forming a continuous distribution view, as shown in Fig. 8C. The horizontal axis represents East Longitude and the vertical axis represents North Latitude. The color scale on the right indicates the electric field strength in dBμV, where warmer colors (red/orange) show higher field intensity, revealing the spatial distribution characteristics and intensity variations of the interference source within the region.

Here, the horizontal axis represents longitude (range: E103.7974° to E103.8041°), and the vertical axis represents latitude (range: N30.8157° to N30.8197°). The radiation intensity of the interference source shows a trend of gradually decreasing from the central area to the surrounding areas. Due to the radiation pattern of the interference source's transmitting antenna and the influence of surrounding environmental factors, the attenuation trend of the interference signal varies in different directions.

3.3. Error Analysis

Possible sources of direction estimation and localization error in this experiment include: electromagnetic interference (EMI), systematic errors, signal and environmental errors, measurement and algorithmic errors, and operational errors.

The field test identified several potential sources of error that impact system performance. First, EMI inherent to the complex UAV platform, while not dominant in this test due to the use of a relatively strong 1 W simulated source, remains a limiting factor for sensitivity and a critical concern for weak signal detection. Other notable error sources are systematic errors arising from antenna array amplitude-phase inconsistencies, installation deviations, and platform-induced pattern disturbances, which necessitate precise future calibration. Signal and environmental errors must also be mitigated, such as multipath propagation over complex terrain and low Signal-to-Noise Ratios (SNR). This will be addressed in future work, by selecting diverse direction-finding points at varying heights and angles, alongside algorithmic enhancements. Furthermore, weak interference detection will benefit from increased antenna gain, optimized LNA performance, or extended signal integration times to improve SNR and reduce noise-induced phase errors. Measurement and algorithmic limitations must also be addressed, including ADC resolution constraints, local oscillator phase noise, and degraded coherent interferometer performance under low SNR or coherent sources. This entails increasing azimuth sampling density and refining coherence coefficient calculations. Finally, operational errors stemming from UAV hovering instability, wind effects, and manual control delays can be minimized by installing higher-precision GPS and developing automated flight algorithms to ensure consistent data acquisition.

4. SUMMARY

This paper introduces a drone-based interference source localization and electromagnetic situation analysis system, aiming to solve the challenge of locating low-power interference sources that affect radio astronomical observations. The system adopts zero-Intermediate Frequency (zero-IF) reception technology and coherent interferometry, enabling monitoring across the 1.1–2 GHz frequency band and accurate localization of interference sources. Due to the design bandwidth of the AD9361 chip and the antenna array, the system theoretically supports real-time monitoring within the 100 MHz–6 GHz frequency band. After subsequent algorithm optimization and error reduction, we will conduct tests at lower and higher frequency bands to achieve wideband real-time monitoring from 100 MHz to 6 GHz. Leveraging the flexibility and mobility of the drone platform, the system can quickly locate interference sources in complex terrains and generate electromagnetic situation maps to determine the interference coverage.

Field tests demonstrate that the system achieves an interference source localization accuracy better than 5°. Beyond precise localization, it can also measure the radiation of interference sources to plot electromagnetic situation maps. This provides robust data support for the identification and localization of interference sources in radio astronomy operations, as well as the planning and management of radio protection zones.

ACKNOWLEDGEMENTS

This work was supported by the following funds: the Special Project for Building a Science and Technology Innovation Center Facing South and Southeast Asia Yunnan Provincial International Joint Innovation Platform: "Yunnan Provincial China-Malaysia International Joint Laboratory of Advanced Radio Astronomy Technology at HF-VHF Bands" (202303AP140003); Advanced Array Technology Research and Development for Space Electromagnetic Sensing on the Technology "Compact Team" Talent Project, the Technology "Compact Team" Talent Project of Urumqi "Hongshan Science Innovation Talent" Cluster Program (B241018006); the Cultivation Project of

Joint Fund for Astronomy under the National Natural Science Foundation of China (U2031133); the SKA Special Project of the Ministry of Science and Technology of the People's Republic of China (2020SKA0110202); the International Partnership Program of the Bureau of International Cooperation, Chinese Academy of Sciences: "Belt and Road" Cooperation (114A11KYSB20200001); the Kunming Municipal Foreign (International) Cooperation Base Project: "Joint R&D Cooperation Base for Advanced Radio Astronomy Technology between Yunnan Observatories, Chinese Academy of Sciences, and University of Malaya" (GHJD-2021022); the Key Special Project "Intergovernmental International Science and Technology Innovation Cooperation" under the National Key R&D Program of the Ministry of Science and Technology of the People's Republic of China: "China-Malaysia Cooperative Research on Space Remote Sensing and Radio Astronomy Observation of Space Weather at Mid-Low Latitudes" (2022YFE0140000); and the SKA Special Project of the Ministry of Science and Technology of the People's Republic of China-High-Precision Calibration Method for Low-Frequency Radio Interferometric Arrays (2020SKA011 0300). Gratitude is expressed to Yunnan Observatories, Chinese Academy of Sciences, for its support.

AI DISCLOSURE STATEMENT

Grammarly was employed for language and grammar checks within the article. The authors carefully reviewed, edited, and revised the Grammarly-generated texts to their own preferences, assuming ultimate responsibility for the content of the publication.

AUTHOR CONTRIBUTIONS

Hongrui Zhang participated in the review and editing of the manuscript, drafted the original version, and provided the research ideas. Liang Dong and Qiang Xi were responsible for hardware development and assisted in manuscript writing. Lesheng He and Yifeng Qin took charge of the construction of the hardware platform. Shengyang Li and Bin Tian were responsible for providing the interference sources required for field tests. Mudi Li designed the flight routes and collected radio interference signals at different altitudes. Ning Zhang was in charge of collating the test data. All authors have read and approved the final manuscript.

DECLARATION OF INTERESTS

The authors declare no competing interests.

REFERENCES

[1] Zhang, H. Y. 2017. Protection progress on radio astronomy frequencies in China. *Progress in Astronomy*, **35**(4): 473−480. (in Chinese)

[2] Zhao, Q. H., Li, J. B., Zhang, T. 2020. The research on range based location algorithmsin radio interference. *Astronomical Research & Technology*, **17**(4): 446−453. (in Chinese)

[3] Zhang, H. Y., Hu, H. L., Wang, Y., et al. 2022. RFI intelligent monitoring techniques for FAST. *Journal of Tsinghua University (Science and Technology)*, **62**(11): 1780−1788. (in Chinese)

[4] Zhu, K. H., Dong, L., Li, J. F. 2024. High elevation satellite interference source localization based on joint time-frequency difference analysis. *Chinese Journal of Radio Science*, **39**(4): 631−639+657. (in Chinese)

[5] Li, J. 2021. The research and realization of key technology of six-channel phase interferometer direction finding system. Master's thesis, Anhui Jianzhu University. (in Chinese)

[6] Memarian, Z., Majidi, M. 2022. Multiple signals direction finding of IoT devices through improved correlative interferometer using directional elements. In Proceedings of 2022 Sixth International Conference on Smart Cities.

[7] Han, J., Gao, J. 2022. Optimal estimation method for direction finding of multi-baseline interferomter. *Electronic Information Warfare Technology*, **37**(2): 38−43. (in Chinese)

[8] Liu, D. R., Miao, S., Dong, L., et al. 2022. Research on measurement of radio interference source based on four-antenna line array. *Astronomical Research & Technology*, **19**(6): 552−558. (in Chinese)

[9] Geng, L. H., Su, C., Du, J., et al. 2023. Solar radio observing and simulation of shadowing effect. *Astronomical Research & Technology*, **20**(1): 15−23. (in Chinese)

[10] Wang, G. B., Fang, Z. T., Chen, S. D., et al. 2026. Current status and future development trends of low-altitude agricultural technology and equipment. *Journal of Intelligent Agricultural Mechanization*, **7**(2): 51−65. (in Chinese)

[11] Analog Devices. 2024. AD9361 RF Agile Transceiver Data Sheet (Rev. G). Available from www.alldatasheet.com/html-pdf/554225/AD/AD9361/23/1/AD9361.html.

[12] Han, G., Wang, B., Wang, D. L. 2010. The research and realization of correlation interferometer direction finding algorithm based on FPGA. *Application of Electronic Technique*, **36**(7): 76−80. (in Chinese)

[13] Li, J., Gao, H. T., Zheng, X. 2005. Mutual coupling analysis and calibration method of phased array antenna in near field. *Acta Electronica Sinica*, **33**(1): 119−122. (in Chinese)

[14] Ma, R. 2019. The research on direction finding intersection and tracking technology. Master thesis, Huazhong University of Science and Technology. (in Chinese)